Biophysical Journal
Article

Role of cholesterol flip-flop in oxidized lipid bilayers

Phansiri Boonnoy,[1,2] Viwan Jarerattanachat,[2,3,4] Mikko Karttunen,[5,6,7] and Jirasak Wong-ekkabut[1,2,3,8,*]
[1]Department of Physics and [2]Computational Biomodelling Laboratory for Agricultural Science and Technology, Faculty of Science, Kasetsart University, Bangkok, Thailand; [3]Thailand Center of Excellence in Physics, Ministry of Higher Education, Science, Research and Innovation, Bangkok, Thailand; [4]NSTDA Supercomputer Center, National Electronics and Computer Technology Center, National Science and Technology Development Agency, Khlong Luang, Pathumthani, Thailand; [5]Department of Chemistry, [6]Department of Physics and Astronomy, and [7]The Centre for Advanced Materials Research, The University of Western Ontario, London, Ontario, Canada; and [8]Specialized Center of Rubber and Polymer Materials for Agriculture and Industry, Faculty of Science, Kasetsart University, Bangkok, Thailand

ABSTRACT We performed a series of molecular dynamics simulations of cholesterol (Chol) in nonoxidized 1-palmitoyl-2-linoleoyl-*sn*-glycero-3-phosphatidylcholine (PLPC) bilayer and in binary mixtures of PLPC-oxidized-lipid-bilayers with 0–50% Chol concentration and oxidized lipids with hydroperoxide and aldehyde oxidized functional groups. From the 60 unbiased molecular dynamics simulations (total of 161 μs), we found that Chol inhibited pore formation in the aldehyde-containing oxidized lipid bilayers at concentrations greater than 11%. For both pure PLPC bilayer and bilayers with hydroperoxide lipids, no pores were observed at any Chol concentration. Furthermore, increasing cholesterol concentration led to a change of phase state from the liquid-disordered to the liquid-ordered phase. This condensing effect of Chol was observed in all systems. Data analysis shows that the addition of Chol results in an increase in bilayer thickness. Interestingly, we observed Chol flip-flop only in the aldehyde-containing lipid bilayer but neither in the PLPC nor the hydroperoxide bilayers. Umbrella-sampling simulations were performed to calculate the translocation free energies and the Chol flip-flop rates. The results show that Chol's flip-flop rate depends on the lipid bilayer type, and the highest rate are found in aldehyde bilayers. As the main finding, we shown that Chol stabilizes the oxidized lipid bilayer by confining the distribution of the oxidized functional groups.

SIGNIFICANCE Cholesterol has a fundamental role in regulation of membrane structure and maintaining membrane fluidity. It may protect membranes from oxidative attacks by free radicals. This study uses both unbiased and biased molecular dynamics simulations of cholesterol in oxidized bilayers to compute the free energy barriers, flip-flop rates, and flip-flop half-lives. The free energy barrier indicates that cholesterol has a higher flip-flop rate within aldehyde bilayers than in 1-palmitoyl-2-linoleoyl-*sn*-glycero-3-phosphatidylcholine and hydroperoxide bilayers. The rate for cholesterol flip-flop decreases with increasing cholesterol concentration, and the aldehyde bilayers have the highest rates. Moreover, the results show the role of cholesterol in preventing lipid bilayer pore formation caused by oxidative stress. Our studies will potentially help to design more efficient molecules to protect membranes from oxidative stress.

INTRODUCTION

Lipid peroxidation modifies the basic physical properties, dynamics, and morphology of biological membranes. The presence of oxidized lipids, products from lipid peroxidation, can cause, for example, an increase in water or free radical permeability, increase in lipid membrane area, and a decrease in lipid chain ordering, resulting in a significant increase in membrane fluidity. Peroxidation also promotes the formation of lipid microdomains (1–8), and the presence of oxidized products such as shortened chain lipids with an aldehyde, carboxylic acid lipids lead to passive pore formation and membrane destruction (2,8–12).

Previous studies have shown that the main causes of pore formation in oxidized bilayers are 1) the presence of high concentration of oxidized lipid with polar moieties such as aldehyde or carboxylic groups at the oxidized lipid chain, and 2) an initial pore formed by those oxidized functional groups that can widely distributed within the bilayer and introduce water into the lipid bilayer (8,10,13,14). Although oxidation is typically seen as detrimental effect, controlled and selective induction of lipid peroxidation in cell membranes has received interest in the context of plasma oncology, a new cancer treatment using cold atmospheric pressure plasma. Cold atmospheric pressure plasma has been shown to be a potential new promising treatment for

Submitted March 6, 2021, and accepted for publication August 26, 2021.
*Correspondence: jirasak.w@ku.ac.th
Editor: Sarah Veatch.
https://doi.org/10.1016/j.bpj.2021.08.036

killing tumor cells by inducing massive lipid peroxidation in the cell membrane, resulting in a pore, a collapse of the membrane, and cell death (15–18).

Cholesterol has a fundamental role in regulation of membrane structure and maintaining membrane fluidity. In the context of oxidized lipids, Van der Paal et al. (11) have shown that an increasing cholesterol fraction in aldehyde-containing bilayers can prevent pore formation and bilayer deformation. The hypotheses for how cholesterol protects a bilayer are related to 1) cholesterol's ability to form hydrogen bonds with oxidized phospholipids and consequent decrease in water permeability through the membrane (19), 2) cholesterol-induced increases in bilayer thickness and lipid chain order parameter (11,13,19,20), 3) cholesterol's geometric shape that complements the conical shape of the oxidized lipids and protects the membrane from collapsing (21), and 4) rapid cholesterol flip-flops helping to relax the stress due to the asymmetrical shape of the oxidized membrane leaflet (22). The rate and mechanism of cholesterol flip-flop have been investigated in various model membranes (23–28). However, its rate in oxidized lipid bilayers remains unknown. Interestingly, cholesterol is also considered to be an antioxidant molecule (29,30). Free energy calculations have indicated that cholesterol has a significant effect on the permeation of reactive species across membranes: it increases the free energy barrier for certain reactive nitrogen oxide species and thus hinders their translocation into the lipid bilayer (31). This protects membranes from oxidative attacks by free radicals. Structurally, both cholesterol and the well-known antioxidant molecule α-tocopherol (α-toc; a form of vitamin E) contain a hydrocarbon chain and a ring structure with a hydroxyl group. This suggests that cholesterol may behave similarly to α-toc in oxidized membranes.

We have previously demonstrated that the presence of high concentrations of α-toc could inhibit pore formation in oxidized lipid bilayers: α-tocs trapped the aldehyde groups at the membrane-water interface, resulting in a decreased water permeability and decreased probability for pore creation (14). In addition, α-tocs have been found to potentially flip-flop more in oxidized lipid bilayer as compared with nonoxidized lipid bilayer. This behavior is also important in how α-toc stabilizes membranes under oxidative stress (14,32). In an independent study, Schumann-Gillett and O'Mara (13) have shown that the presence of cholesterol disturbs the orientation of the oxidized *sn*-2 chain of 1-palmitoyl-2-(9′-oxo-valeroyl)-*sn*-glycero-3-phosphocholine by pushing the aldehyde functional group to move forward to the membrane-water interface. Because of the limited simulation time and low concentrations of oxidized lipids, they observed neither pore formation induced by oxidized lipids nor cholesterol flip-flops in 500-ns molecular dynamics (MD) simulations, thus leaving the question about the physical mechanism of how cholesterol inhibits pore formation in oxidized lipid bilayers unresolved. Their observations do, however, suggest that α-toc and cholesterol may, at least qualitatively, use a similar mechanism for preventing pore formation in oxidized lipid bilayers.

It is also well known that increasing the fraction of cholesterol in a membrane induces a lipid phase transition from the liquid-disordered (L_d) to the liquid-ordered (L_o) phase in nonoxidized lipid bilayers (33–36) associated with lipid raft microdomains in membranes (33,36–41). These have been implicated in cell signaling and membrane trafficking (42,43). Previous studies have focused on the effect of cholesterol on nonoxidized bilayers (36,39,41,44), but how cholesterol induces ordered phase in oxidized phospholipid bilayers remains unknown.

The aims of this work are to investigate the behavior of cholesterol flip-flop and the effect of lipid phase transition induced by cholesterol in both nonoxidized and oxidized lipid bilayers. We performed a series of systematic MD simulations by varying the cholesterol concentration (0–50%) in pure 1-palmitoyl-2-linoleoyl-*sn*-glycero-3-phosphatidylcholine (PLPC) bilayers and in binary mixtures of PLPC and its four main oxidative products. Free energy barriers for a cholesterol translocating in lipid bilayers and cholesterol flip-flop rates were estimated to understand cholesterol flip-flop in the different systems.

MATERIALS AND METHODS

Unbiased MD simulations

To investigate the behavior of cholesterol in the PLPC and oxidized-PLPC lipid bilayers, a series of MD simulations of cholesterol in PLPC bilayers and binary mixtures with 1:1 ratio of PLPC/PLPC's oxidation products were performed. The four main oxidation products of PLPC, namely 1-palmitoyl-2-(13-hydroperoxy-*trans*-11,*cis*-9-octadecadienoyl)-*sn*-glycero-3-phosphocholine (13-tc), 1-palmitoyl-2-(9-hydroperoxy-*trans*-10, *cis*-12-octadecadienoyl)-*sn*-glycero-3-phosphocholine (9-tc), 1-palmitoyl-2-(12-oxo-*cis*-9-dodecenoyl)-*sn*-glycero-3-phosphocholine (12-al), and 1-palmitoyl-2-(9-oxo-nonanoyl)-*sn*-glycero-3-phosphocholine (9-al), were used. Chemical structures of cholesterol and lipids are shown in Fig. 1. The structures and force field parameters of 1) PLPC and oxidized lipids were taken from previous studies (1,3,10,32,45), and 2) cholesterol from Höltje et al. (46). All systems were generated using the MemGen program (47). Full descriptions of the simulation systems are shown in Table S1.

After energy minimization with the steepest descents algorithm, MD simulations were run for 1–3 μs with an integration time step of 2 fs by using the GROMACS 5.1.2 program package (48). All simulations were performed under the constant of the number of atoms, pressure, and temperature (NPT) ensemble. The temperature was set to 298 K by the velocity-rescaling algorithm (49) with a time constant of 0.1 ps. Semi-isotropic pressure was applied using the Parrinello-Rahman algorithm (50) with a time constant of 4.0 ps and compressibility of 4.5×10^{-5} bar^{-1} to keep a constant pressure at 1 bar. All bond lengths were constrained by the parallel linear constraint solver (P-LINCS) algorithm (51). Periodic boundary conditions were applied in all three dimensions, and the neighbor list was updated at every integration time step (52). A cutoff value of 1.0 nm was used for the real space part of van der Waals and electrostatic interactions. The particle-mesh Ewald method (53–55) was applied to compute the long-rang electrostatic interactions with a 0.12-nm grid in the reciprocal-space interaction and cubic interpolation of order 4. The last 500 ns were used for data analysis. For the bilayers with a pore, the last 50 ns before pore formation were used for analysis. Statistical errors were estimated based on standard deviation. The

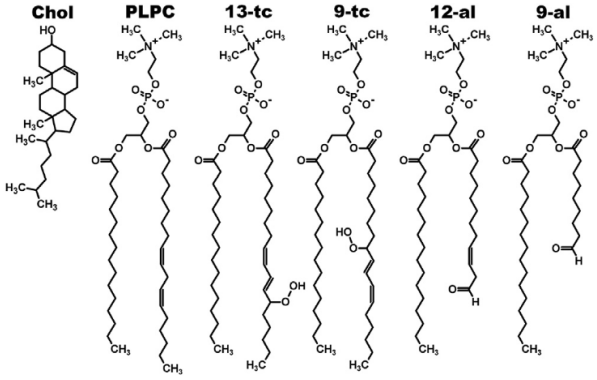

FIGURE 1 Chemical structures of cholesterol, PLPC, and its four main oxidative products, hydroperoxide (*13-tc* and *9-tc*), and aldehyde lipids (*12-al* and *9-al*).

simulation protocol has been previously validated and used to study several biomolecular interactions such as lipid-lipid interactions, carbon-nanoparticle-matrix interactions, membrane transport, and protein-DNA-drug interactions, including drug delivery systems (56–62). Visual Molecular Dynamics (63) was used for visualizations.

Umbrella-sampling MD simulations

Biased umbrella-sampling MD simulations (64) with the Weighted Histogram Analysis Method (65) were performed to investigate the potential of mean force (free energy profile) for a cholesterol molecule partitioning across the 100% PLPC, 50% 13-tc, 50% 9-tc, 50% 12-al, and 50% 9-al lipid bilayers. The free energy profile allows for estimation of the free energy barrier for cholesterol flip-flop. A series of 26 simulation windows with varying positions of cholesterol were performed to compute the free energy profiles. Cholesterol was moved from the bilayer center (at z = 0 nm) to the lipid-water interface (at z = 2.5 nm) with 0.1-nm increments per window. During the umbrella-sampling MD simulations, cholesterol's hydroxyl group (see Fig. 1) was restrained in the z-direction using a harmonic potential function with a force constant of 3000 kJ/(mol nm^2). All simulations were run under the NPT ensemble at the temperature of 298 K and pressure of 1 bar. MD simulations were performed for at least 100 ns, and the last 50 ns was used for analysis. The last 50 ns from umbrella-sampling simulation was divided into 10 intervals. The averages were calculated for the potential of mean force profiles, and statistical errors of free energy were estimated using standard error (66).

Calculation of cholesterol flip-flop rate

To calculate the flip-flop rate (k_{flip}), we performed additional 250 unbiased MD simulations of cholesterol in 100% PLPC, 50% 13-tc, 50% 9-tc, 50% 12-al, and 50% 9-al lipid bilayers. The initial configurations of each system were taken from the structures at 100 ns of the umbrella-sampling MD simulations in which the cholesterol's hydroxyl group was located at the bilayer center. After removing the harmonic restraint, the 50 independent unbiased MD simulations of each lipid bilayer were independently run for 50–300 ns. We measured the time for the hydroxyl group of cholesterol to move from the bilayer center to the equilibrium position (t_d) and calculated the rate for cholesterol flip-flop (k_{flip}) using (24,26)

$$k_{flip} = \frac{1}{\left[\left(1/k_f\right) + \left(1/k_d\right)\right]} \times 1/2, \quad (1)$$

where $k_d = 1/t_d$ is the rate at which cholesterol moves from the bilayer center to the equilibrium position. The rate for cholesterol to move from the equilibrium position to the bilayer center (k_f) was calculated using

$$k_f = k_d \times \exp\left(-\Delta G_{barrier}/RT\right), \quad (2)$$

where $\Delta G_{barrier}$ is the energy barrier for cholesterol flip-flop. R and T are the gas constant and temperature, respectively. The half-life for cholesterol flip-flop ($t_{1/2}$) is then given as

$$t_{1/2} = \ln 2/k_{flip}. \quad (3)$$

RESULT AND DISCUSSION

Summary of the membrane structures is shown in Table 1, and Figs. S1–S5 show snapshots of the systems. Without cholesterol, no pore formation was observed in 100% PLPC and 50% hydroperoxide-containing oxidized bilayers (50% 13-tc and 50% 9-tc), whereas stable pores were observed in the 50% aldehyde-containing oxidized bilayers (50% 12-al and 50% 9-al). These results agree well with previous MD simulation studies that have shown that aldehyde lipids at high concentrations (>50%) are capable of inducing pore formation (2,10,11,14,32).

The presence of cholesterol appears to inhibit pore formation in the 50% aldehyde-containing oxidized bilayers: although pores were observed at low cholesterol concentrations (1.5–6%), pore formation did not occur at higher concentrations (>11%) during the 3-μs simulations. Recent computational simulation studies (11,19) have suggested that at least 16 and 30% cholesterol is required to inhibit pore formation in pure aldehyde and mixtures of aldehyde/carboxylic oxidized bilayers, respectively; the concentration of cholesterol necessary to inhibit pore formation in an oxidized membrane depends on the lipid composition.

TABLE 1 Simulated systems and membrane structures

	Cholesterol concentration											
System	0%	1.5%	3%	6%	11%	17%	20%	23%	29%	33%	40%	50%
100% PLPC	×	×	×	×	×	×	×	×	×	×	×	×
50% 13-tc	×	×	×	×	×	×	×	×	×	×	×	×
50% 9-tc	×	×	×	×	×	×	×	×	×	×	×	×
50% 12-al	pore	pore	pore	pore	✓	✓	×	×	×	×	×	×
50% 9-al	pore	pore	pore	pore	✓	✓	✓	✓	×	×	×	×

The cross mark (×) indicates that no cholesterol flip-flops were observed. The check mark (✓) indicates that flip-flops were observed. The phase states of bilayers were reported in Table S1.

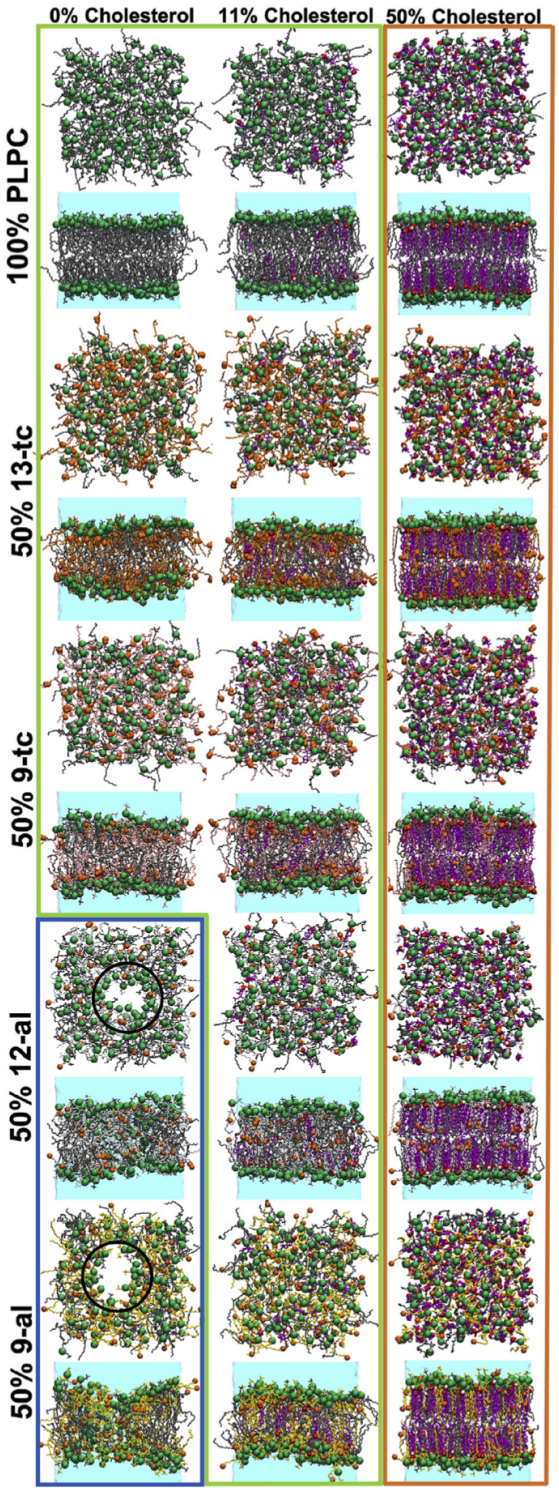

FIGURE 2 Top- and side-view snapshots of the lipid bilayers: at 0% cholesterol, the 100% PLPC bilayer and the 50% hydroperoxide bilayers are in the L_d phase. The 50% aldehyde-containing oxidized bilayers are in the L_d phase and have a pore. The open black circle indicates a water pore in bilayer. At 11 and 50% cholesterol, the lipid bilayers are in the L_d and L_o phases, respectively. Blue, green and orange boxes represent the bilayers in L_d phase with a pore, L_d phase, and L_o phase, respectively. The light blue surface represents the water region. Phosphorus atoms in lipid headgroups are shown as green spheres. The lipid chains of PLPC, 13-tc, 9-tc, 12-al, 9-al, and cholesterol are shown in gray, orange, pink, white, yellow, and purple (chains), respectively. The oxidized functional groups are displayed as orange spheres. Cholesterols' hydroxyl groups are shown in red and white spheres representing oxygen and hydrogen atoms, respectively. To see the figure in color, go online.

Visualizations of trajectories showed rapid flip-flops of cholesterol between leaflets only for the 50% aldehyde bilayers (50% 12-al and 50% 9-al) at cholesterol concentrations 11–23%. Furthermore, increasing cholesterol concentration led to a phase state change from an L_d phase to an L_o phase as shown in Fig. 2 and Table S1. This was observed for all bilayers. The L_o phase appeared at higher cholesterol concentrations in the presence of oxidized lipids.

Effects of cholesterol on the density distribution of the oxidized *sn*-2 chain in the bilayer

We analyzed the mass density of the oxidized functional groups along the z-direction (bilayer normal) using distance from the bilayer center. The bilayer center is defined as the center of mass of the lipid bilayer. The mass density profiles are symmetrized of the upper and lower leaflets and are shown in Fig. 3.

Mass density profiles of the hydroperoxide group in 50% 13-tc and 50% 9-tc bilayers

In the absence of cholesterol, the preferential location of the hydroperoxide group in the 50% 13-tc and 50% 9-tc is near the lipid-water interface. This is consistent with previous experimental and computational studies (6,10,67,68). When increasing cholesterol concentration, the peak of the density distribution shifts slightly toward the lipid-water interface as the bilayer thickness increases (Fig. 3, *A* and *B*).

The above behavior changes at a certain cholesterol concentration (29% for 13-tc and 40% for 9-tc). The addition of cholesterol induces a reduction in the density of the hydroperoxide functional groups at the lipid-water interface, whereas their density at the bilayer center becomes larger. At 40 and 50% cholesterol concentrations, qualitative differences between the 50% 13-tc and 50% 9-tc bilayers were observed. In the 50% 13-tc bilayer, there are two peaks with the maximum occurring near the bilayer center and the second peak near the lipid-water interface (Fig. 3 *A*). In contrast, in the 50% 9-tc bilayer, however, the distribution of hydroperoxide group consists of three peaks: 1) at about the lipid-water interface, 2) below the carbonyl group, and 3) at ~0.5 nm from the bilayer center (Fig. 3 *B*).

Mass density profiles of the aldehyde group in 50% 12-al and 50% 9-al bilayers

Up to cholesterol concentrations of 23% in 12-al and 29% in 9-al, the aldehyde group of the oxidized *sn*-2 chain had a

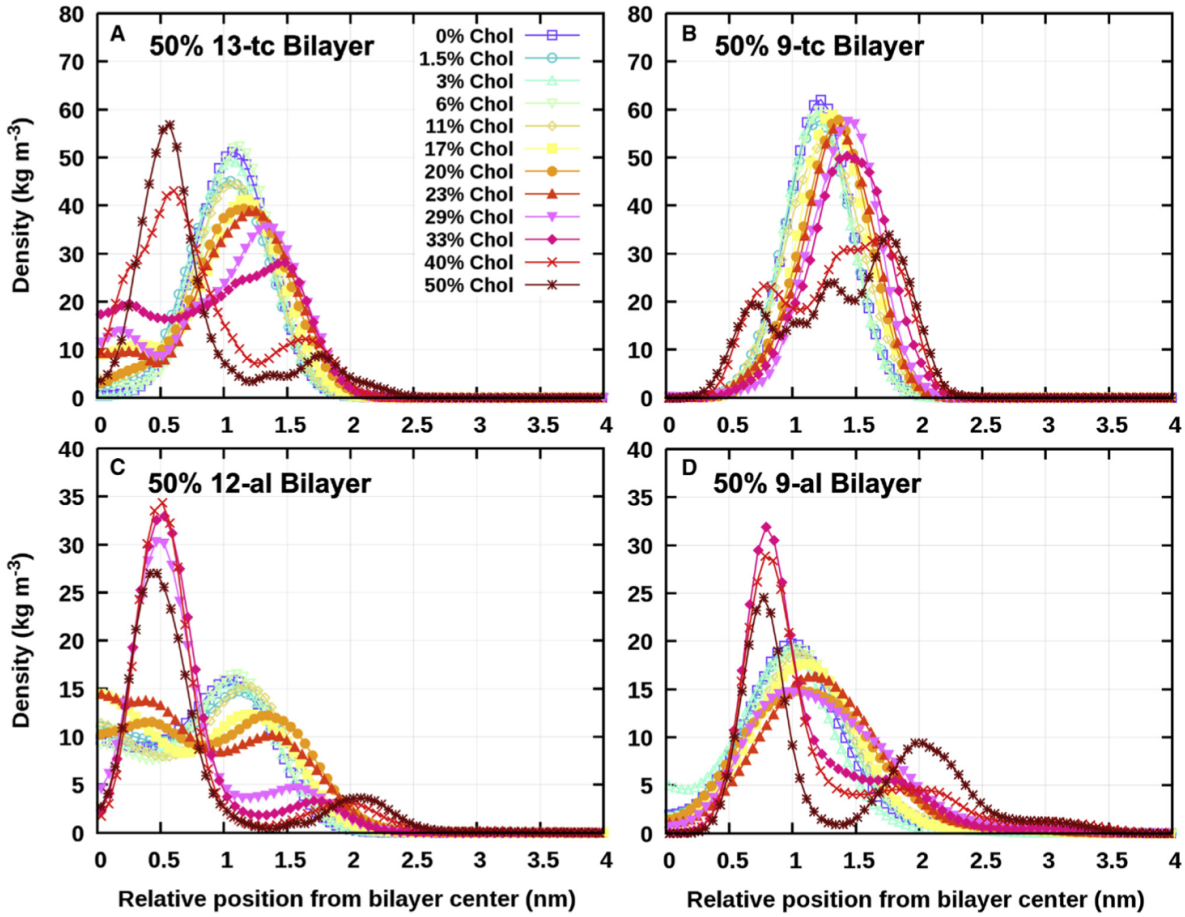

FIGURE 3 Density distributions of the oxidized functional groups (see Fig. 1 for structures) along the z axis with respect to the distance from the bilayer center at different cholesterol concentrations. The mass density profiles are symmetrized. Shown are the hydroperoxide functional group in the case of 13-tc (*A*) and 9-tc (*B*) and aldehyde functional group in the case of 12-al (*C*) and 9-al (*D*). To see the figure in color, go online.

wide distribution across the bilayer (Fig. 3, *C* and *D*). Upon addition of cholesterol, however, the maximum at the lipid-water interface decreases, whereas the density at the bilayer center increases. Above these concentrations, the bilayer is in the L_o phase, and the density maximum shifts from the lipid-water interface to the bilayer interior (~0.8 nm from the bilayer center), but broad peak at the lipid-water interface is still observed. As discussed in our previous MD simulation study (10), the orientation and broad distribution of aldehyde within the oxidized bilayer are the main mechanisms of how aldehyde lipids increase water permeability and induce pore formation.

Further addition of cholesterol leads to a qualitative change in the distribution. This behavior directly affects the aldehyde lipids' ability to induce pore formation (10) and appears to be the same as how α-toc inhibits pore formation in aldehyde bilayers (14). In addition, the increase in the amplitude of the peak near the bilayer center indicates that the *sn*-2 chain points toward the bilayer center. Our previous MD simulations have demonstrated that the distribution of oxidized lipid chains determines the lipid shape and plays an essential role in self-assembly: 12-al and 9-al lipid taking the shape of truncated cones usually self-aggregate to induce a pore in the lipid bilayer, and they form micellar structure, whereas PLPC, 13-tc, and 9-tc lipids taking cylindrical shapes typically form bilayers (10,69). These imply that at high cholesterol concentrations, aldehyde lipids undergo a significant geometrical change from a truncated cone to a cylindrical shape, helping to prevent pore formation and making the lipid bilayer structure more stable.

Cholesterol flip-flop rate

It has been previously suggested (22) that rapid cholesterol flip-flops may protect membranes by balancing the area and relaxing differential-density stress in a symmetrical oxidized lipid membrane. We observed spontaneous cholesterol flip-flops in the 50% 12-al bilayer containing 11 and

17% of cholesterol and in the 50% 9-al bilayers containing 11, 17, 20, and 23% of cholesterol. In these cases, one to three cholesterol molecules flipped between the two leaflets, and each of those molecules underwent a single flip-flop only. For the 100% PLPC and 50% hydroperoxide (13-tc and 9-tc) bilayers, no cholesterol flip-flops were observed during 3 μs. To the best of our knowledge, cholesterol flip-flop rates in oxidized lipid bilayers have not yet been elaborated. To do that, we first performed umbrella-sampling MD simulations to calculate the free energy barriers and then calculated the cholesterol flip-flop rates in the different oxidized lipid bilayers.

Free energy profiles

The free energy profiles for moving a cholesterol molecule from the bilayer center to the lipid-water interface are shown in Fig. 4, and the associated thermodynamic properties are listed in Table 2. In the profiles, the position of the minimal free energy represents the equilibrium position of the hydroxyl group of cholesterol molecule with respect to the distance from bilayer center. The free energy barrier ($\Delta G_{barrier}$) is the maximum in free energy inside the bilayer for moving a cholesterol from the equilibrium position to the bilayer center. The free energy profiles were calculated using the Weighted Histogram Analysis Method tool in the GROMACS package.

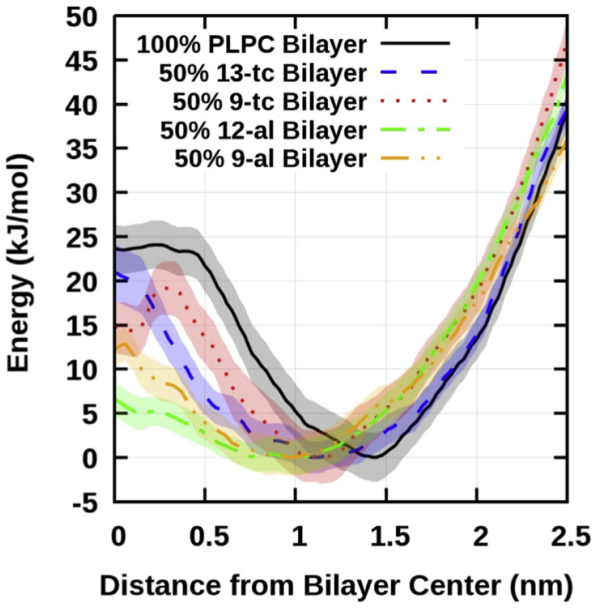

FIGURE 4 Free energy profiles of cholesterol molecule flip-flop across the 100% PLPC and 50% oxidized-PLPC bilayers. The free energy was set equal to zero at the equilibrium position of the hydroxyl group of cholesterol in the bilayer. Error bars were estimated using the standard error as described in Umbrella-sampling MD simulations. Fig. S6 shows the free energy profiles with the errors computed by the commonly used bootstrap method (70). To see the figure in color, go online.

TABLE 2 Thermodynamic properties for moving a cholesterol molecule across the 100% PLPC and 50% oxidized-PLPC bilayers

System	$\Delta G_{barrier}$ (kJ/mol)	Equilibrium position (nm)
100% PLPC	24.09 ± 3.83	1.40 ± 0.02
50% 13-tc	21.40 ± 3.62	1.12 ± 0.05
50% 9-tc	19.15 ± 4.26	1.12 ± 0.03
50% 12-al	6.85 ± 2.61	0.89 ± 0.06
50% 9-al	12.86 ± 2.80	0.99 ± 0.03

$\Delta G_{barrier}$ is the free energy for moving a cholesterol molecule from its equilibrium position to the bilayer center. Equilibrium position is measured with respect to the distance from the bilayer center.

In 100% PLPC bilayer, the equilibrium position of cholesterols' hydroxyl groups was found to be 1.40 ± 0.02 nm from the bilayer center. This position is related to the location of the lipids' carbonyl groups. The average distance of the carbonyl group from the bilayer center is 1.48 ± 0.03 nm. The result implies that the hydroxyl group of cholesterol prefers to stay at the lipid-water interface close to the carbonyl group in the 100% PLPC bilayer. In the 50% oxidized lipid bilayers, the equilibrium positions of cholesterols' hydroxyl groups were observed to be deeper inside the bilayer than in the pure PLPC bilayer at the distances of 1.12 ± 0.05, 1.12 ± 0.03, 0.89 ± 0.06, and 0.99 ± 0.03 nm from bilayer center for 50% 13-tc, 50% 9-tc, 50% 12-al, and 50% 9-al, respectively. This results from the decrease of bilayer thickness in the presence of oxidized lipids. In addition, the location of the cholesterol hydroxyl group remains in the bilayer interior under the lipid carbonyl groups. The average distances of the lipid carbonyl groups from the bilayer center are 1.31 ± 0.03, 1.34 ± 0.03, 1.23 ± 0.03, and 1.18 ± 0.16 nm for 50% 13-tc, 50% 9-tc, 50% 12-al, and 50% 9-al, respectively.

The free energy barrier ($\Delta G_{barrier}$) for cholesterol flip-flop between leaflets in 100% PLPC bilayer is ∼24.09 ± 3.83 kJ mol^{-1}. For a comparison, in 1-palmitoyl-2-oleoyl-*sn*-glycero-3-phosphocholine bilayer, $\Delta G_{barrier}$ has been reported to be ∼23–29 kJ mol^{-1} (24–26) and ∼21.5–27 kJ mol^{-1} in 1,2-dipalmitoyl-*sn*-glycero-3-phosphocholine (DPPC) bilayer (24,25,71). The slight differences in $\Delta G_{barrier}$ might depend on the type of lipid as well as temperature (24,72). Compared with 100% PLPC, in 50% hydroperoxide bilayers, the free energy barrier decreases only slightly: in 50% 13-tc, the barrier was determined to be 21.40 ± 3.62 kJ mol^{-1} and in 50% 9-tc $\Delta G_{barrier}$ = 19.15 ± 4.26 kJ mol^{-1}. In the cases of 50% aldehyde lipids, the changes are more dramatic: $\Delta G_{barrier}$ = 6.85 ± 2.61 kJ mol^{-1} for 50% 12-al and $\Delta G_{barrier}$ = 12.86 ± 2.80 kJ mol^{-1} for 50% 9-al. These results suggest that the probability for cholesterol flip-flop within the aldehyde-containing oxidized bilayer is higher than the hydroperoxide-containing oxidized bilayer and the nonoxidized-PLPC bilayer consistent with the data of cholesterol flip-flop in the lipid bilayer from the unbiased MD simulations (Table 1).

We have compared the results of t_d and the reorientation time in the unbiased simulations of 50% 9-al bilayer containing 11% (Fig. S7 *A*) and 17% (Fig. S7 *B*) cholesterol. However, only one cholesterol flip-flop event was observed in each system, and thus, these results should be considered as very much qualitative rather than quantitative. The results indicate that the reorientation timescale is very rapid compared with t_d.

The thermodynamic and kinetic properties for cholesterol flip-flop are shown in Table 3. To obtain the statistical significance in $\bar{k}_{flip}$, the standard deviations for the average rates of cholesterol flip-flop ($\bar{k}_{flip}$) were calculated, and the results are shown in Table 3. In addition, to compare the differences in $\bar{k}_{flip}$ among lipid types, the *p*-values of k_{flip} were calculated using the *t*-test (see Table S2). The results indicate that the average rate of cholesterol flip-flop ($\bar{k}_{flip}$) in 50% oxidized lipid bilayers is higher than in the PLPC bilayer. In the 100% PLPC bilayer, $\bar{k}_{flip}$ is approximately $(3.0 \pm 2.5) \times 10^3\ s^{-1}$. In the 50% hydroperoxide-containing oxidized bilayers, $\bar{k}_{flip}$ were found to be $(3.4 \pm 3.8) \times 10^3\ s^{-1}$ for 50% 13-tc bilayer and $(3.3 \pm 3.4) \times 10^4\ s^{-1}$ for 50% 9-tc bilayer. Although no significant increase in $\bar{k}_{flip}$ was observed in the 50% 13-tc bilayer as compared with the 100% PLPC bilayer, an increase by an order of magnitude was observed in the 50% 9-tc bilayer. This implies that the position of the hydroperoxide group in the oxidized lipid chain may influence cholesterol flip-flop in the oxidized bilayer. In the 50% aldehyde-containing oxidized bilayer, $\bar{k}_{flip}$ had a rate higher by one to three orders of magnitude compared with the 100% PLPC and the hydroperoxide-containing oxidized bilayer. The values for $\bar{k}_{flip}$ were found to be $(3.2 \pm 3.7) \times 10^6\ s^{-1}$ for 50% 12-al bilayer and $(4.5 \pm 4.8) \times 10^5\ s^{-1}$ for 50% 9-al bilayer. The results suggest that the cholesterol flip-flop rate depends on the bilayer type, and the highest flip-flop rate is found in the aldehyde-containing oxidized bilayer.

Using MD simulations, Bennett et al. (24) found that the cholesterol flip-flop rate in the long-chain 1,2-diarachidonoyl-*sn*-glycero-3-phosphatidylcholine (20:4-20:4 phosphatidylcholine) bilayer was an order of magnitude higher than in the DPPC (16:0-16:0 phosphatidylcholine) bilayer and suggests faster cholesterol flip-flop in less-ordered membranes with polyunsaturated 1,2-diarachidonoyl-*sn*-glycero-3-phosphatidylcholine lipids. They also reported that k_{flip} of cholesterol decreased when cholesterol concentration increased from 0 to 40% in a DPPC bilayer. An increase in cholesterol concentration from 0 to 40% in a DPPC bilayer could lead to a lipid phase transition from L_d to the L_o (73,74). The above implies that adding cholesterol in the DPPC bilayer results in an increase in membrane packing and a consequent decrease in cholesterol flip-flop. In addition, Gu et al. (28) have reported that a decrease in temperature from 310 to 290 K results in an increase in lipid chain packing in a ternary DPPC-1,2-dioleoyl-*sn*-glycero-3-phosphocholine-cholesterol-mixture. This was shown to lead to a significant decrease by approximately an order of magnitude in cholesterol flip-flop events. The observed decrease in the flip-flop rate is fully consistent with the well-known condensing effect of cholesterol (72,75).

Effects of cholesterol on the physical properties of oxidized-PLPC bilayers

The analyses of mass density profiles show that the hydroxyl groups of cholesterol (i.e., cholesterol headgroup) are at the lipid-water interface and that the cholesterols' terminal methyl groups (i.e., cholesterol tail) extend toward the bilayer center (see Figs. S8–S12).

The average distance from the bilayer center to 1) the hydroxyl groups of cholesterol, 2) lipids' phosphorus atoms, and 3) lipids' carbonyl groups were calculated to investigate their relative positions in the bilayer. The results in Fig. 5 and Table S3 show that the hydroxyl group of cholesterol prefers to be located below the lipid carbonyl groups, when the bilayer is in the L_d phase. It is consistent with the equilibrium position of cholesterols' hydroxyl groups from the free energy calculation (Fig. 4). Upon increasing cholesterol concentration, the cholesterol headgroup moves closer to the lipid-water interface, with the hydroxyl group of cholesterol interacting with the lipid headgroup. The average bilayer thickness (Fig. 6) was obtained as the distance between the phosphorus atoms. For all lipid bilayers, the addition of cholesterol leads to an increase in bilayer thickness.

TABLE 3 Cholesterol flip-flop in the different lipid bilayers

System	t_d (ns)	Average t_d (ns)	k_d (s^{-1})	k_f (s^{-1})	$\bar{k}_{flip}$ (s^{-1})	$t_{1/2}$ (s)
100% PLPC	2.5–56.1	16.4 ± 11.2	4.0×10^8 to 1.8×10^7	2.4×10^4 to 1.1×10^3	$(3.0 \pm 2.5) \times 10^3$	$(3.8 \pm 2.6) \times 10^{-4}$
50% 13-tc	4.0–215.4	48.8 ± 34.5	2.5×10^8 to 4.6×10^6	4.5×10^4 to 8.3×10^2	$(3.4 \pm 3.8) \times 10^3$	$(3.8 \pm 2.7) \times 10^{-4}$
50% 9-tc	1.1–41.2	11.4 ± 8.0	9.5×10^8 to 2.4×10^7	4.2×10^5 to 1.1×10^4	$(3.3 \pm 3.4) \times 10^4$	$(3.6 \pm 2.5) \times 10^{-5}$
50% 12-al	1.5–53.1	16.3 ± 10.6	6.8×10^8 to 1.9×10^7	4.3×10^7 to 1.2×10^6	$(3.2 \pm 3.7) \times 10^6$	$(3.8 \pm 2.5) \times 10^{-7}$
50% 9-al	1.2–39.1	7.0 ± 6.2	8.5×10^8 to 2.6×10^7	4.8×10^6 to 1.4×10^5	$(4.5 \pm 4.8) \times 10^5$	$(1.7 \pm 1.5) \times 10^{-6}$

The value of t_d is the time for the hydroxyl group of cholesterol move from the bilayer center to the equilibrium position. The value of k_d is the rate for the hydroxyl group of cholesterol to move from the bilayer center to the equilibrium position; k_d was calculated by $k_d = 1/t_d$. The rate for cholesterol to move from the equilibrium position to the bilayer center (k_f) was calculated by Eq. 2. The rate of cholesterol flip-flops (k_{flip}) was calculated by Eq. 1, and the average rate for cholesterol flip-flop ($\bar{k}_{flip}$) was estimated. The half-life for cholesterol flip-flop ($t_{1/2}$) was calculated by Eq. 3. The errors were estimated using standard deviation.

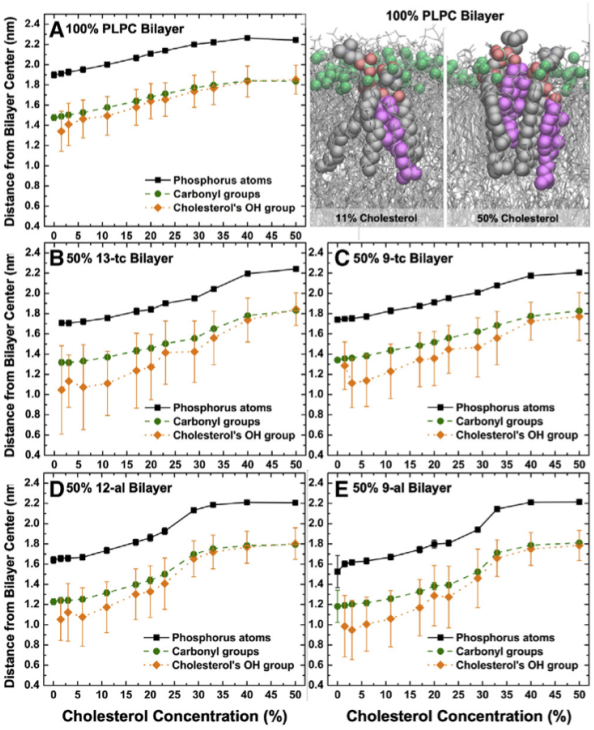

FIGURE 5 Average distance of the lipid phosphorus atoms, carbonyl groups, and cholesterol's hydroxyl group from the bilayer center for 100% PLPC (*A*), 50% 13-tc (*B*), 50% 9-tc (*C*), 50% 12-al (*D*), and 50% 9-al (*E*) bilayer. The snapshot shows an example of the location of cholesterol in the 100% PLPC bilayer at 11 and 50% of cholesterol. Cholesterol is shown in magenta. Phosphorus atoms in the lipid headgroups are displayed as green spheres and PLPC molecules as gray lines. The red and white spheres are oxygen and hydrogen atoms, respectively. To see the figure in color, go online.

At 0% cholesterol concentration, the 100% PLPC bilayer is thicker compared with the 50% oxidized lipid bilayer. Note that all the lipid bilayers at 0% cholesterol are in the L_d phase. For all lipid bilayers, the addition of 1.5–6% cholesterol concentration did not significantly increase thickness. However, increasing cholesterol concentration over 11% led to a significant increase in bilayer thickness compared with the bilayer without cholesterol. At 50% cholesterol concentration, the L_o phase was observed in all lipid bilayers, and no difference in the thicknesses between 100% PLPC bilayer and 50% oxidized lipid bilayer was observed.

To gain understanding of the effect of cholesterol on the elastic properties, we computed the area compressibility modulus (K_A) in all lipid bilayers. K_A was calculated from the fluctuations in the area per lipid using (76)

$$K_A = \frac{k_B T \langle A_L \rangle}{N(\sigma_A)^2}, \quad (4)$$

where k_B and T are the Boltzmann constant and temperature, respectively. $<A_L>$ is the average area per lipid, $(\sigma_A)^2$ is the variance of the area per lipid, and N is the number of lipids per leaflet. The average K_A as a function of cholesterol concentration in the 100% PLPC and 50% oxidized lipid bilayers is shown in Fig. S13. The results showed that in the L_d phase, the addition of cholesterol did not significantly change the area compressibility modulus. However, when the lipid phase state changes from L_d to the L_o phase, a rapid increase in K_A is clearly observed in all bilayers.

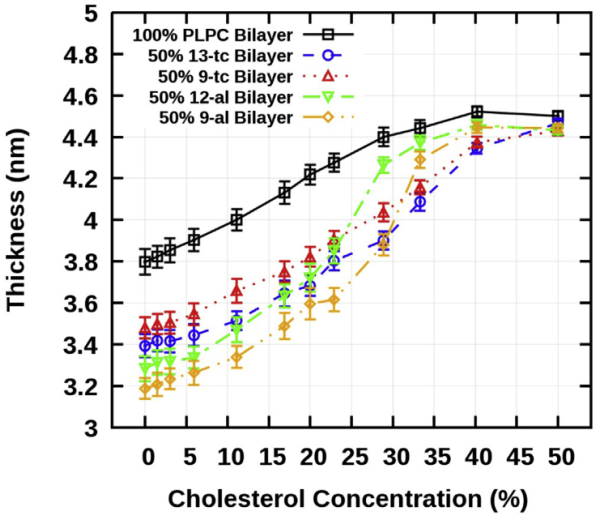

FIGURE 6 Average bilayer thickness of the 100% nonoxidized-PLPC bilayer and 50% oxidized lipid bilayer as a function of cholesterol concentration. The errors were estimated using standard deviation. To see the figure in color, go online.

CONCLUSIONS

We performed 161-μs unbiased MD simulations as well as umbrella-sampling simulations to understand the role of cholesterol in preventing lipid bilayer pore formation caused by oxidative stress. As model systems, we used pure PLPC and 50% binary mixtures of PLPC-oxidized-lipids and varied cholesterol concentration. Without cholesterol, no pore formation was observed for 100% PLPC and 50% PLPC-hydroperoxide-bilayers, whereas a stable pore was observed in the 50% PLPC-aldehyde-bilayers. We found that adding over 11% cholesterol concentrations can prevent pores in aldehyde bilayers. First, we investigated the effect of cholesterol on oxidized chain distribution in the lipid bilayer. The results show that cholesterol restricts the distribution and changes the orientation of the oxidized lipid functional group in the bilayer. This had a direct influence on pore formation in the aldehyde lipid bilayers in which cholesterols confine the distribution of the aldehyde groups, resulting in a decreased probability for pore creation compared with systems without cholesterol (10). It is consistent with the mechanism of how α-tocs inhibited pores in oxidized lipid bilayers in our previous study (14).

Next, we studied cholesterol flip-flop within the bilayer. In the 100% PLPC and 50% hydroperoxide bilayer, no flip-flop events were observed during 3 μs. However, there were one to three flip-flop events within the aldehyde bilayer. To understand the flip-flop behavior in the different bilayers, we performed 130 biased umbrella-sampling MD simulations to calculate the free energy barrier and performed extended unbiased MD simulations to estimate the rate for cholesterol flip-flop. The free energy barrier indicates that flip-flops are more favorable within the aldehyde bilayer as compared with the PLPC and hydroperoxide bilayers. The rate for cholesterol flip-flop decreases with increasing cholesterol concentration, the highest rate being in the aldehyde bilayer. Systematic analyses were carried out to describe the changes caused by varying concentrations of cholesterol in oxidized lipid bilayers. We found that cholesterols induce tighter lipid packing, resulting in inhibition of membrane damage. This work improves our understanding toward the interplay between cholesterols and oxidized lipids and can potentially be applied for improving cold plasma treatments of tumors (17,77).

SUPPORTING MATERIAL

Supporting material can be found online at https://doi.org/10.1016/j.bpj.2021.08.036.

ACKNOWLEDGMENTS

Computing facilities were provided by SHARCNET (www.sharcnet.ca), Compute Canada (www.computecanada.ca), and the Department of Physics, Faculty of Science, Kasetsart University.

This work was financially supported by the National Research Council of Thailand, Thailand Science Research and Innovation, through the Research Grants for Talented Mid-Career Researchers grant no. N41A640080 and the Royal Golden Jubilee Ph.D. Program grant no. PHD/0204/2559 (to J.W.-e. and P.B.). M.K. thanks the Natural Sciences and Engineering Research Council of Canada and the Canada Research Chairs Program for financial support.

REFERENCES

1. Wong-Ekkabut, J., Z. Xu, …, L. Monticelli. 2007. Effect of lipid peroxidation on the properties of lipid bilayers: a molecular dynamics study. *Biophys. J.* 93:4225–4236.
2. Lis, M., A. Wizert, …, L. Cwiklik. 2011. The effect of lipid oxidation on the water permeability of phospholipids bilayers. *Phys. Chem. Chem. Phys.* 13:17555–17563.
3. Jarerattanachat, V., M. Karttunen, and J. Wong-Ekkabut. 2013. Molecular dynamics study of oxidized lipid bilayers in NaCl solution. *J. Phys. Chem. B.* 117:8490–8501.
4. Weber, G., T. Charitat, …, A. P. Schroder. 2014. Lipid oxidation induces structural changes in biomimetic membranes. *Soft Matter.* 10:4241–4247.
5. Runas, K. A., and N. Malmstadt. 2015. Low levels of lipid oxidation radically increase the passive permeability of lipid bilayers. *Soft Matter.* 11:499–505.
6. Guo, Y., V. A. Baulin, and F. Thalmann. 2016. Peroxidised phospholipid bilayers: insight from coarse-grained molecular dynamics simulations. *Soft Matter.* 12:263–271.
7. Tsubone, T. M., M. S. Baptista, and R. Itri. 2019. Understanding membrane remodelling initiated by photosensitized lipid oxidation. *Biophys. Chem.* 254:106263.
8. Tsubone, T. M., H. C. Junqueira, …, R. Itri. 2019. Contrasting roles of oxidized lipids in modulating membrane microdomains. *Biochim. Biophys. Acta Biomembr.* 1861:660–669.
9. Cwiklik, L., and P. Jungwirth. 2010. Massive oxidation of phospholipid membranes leads to pore creation and bilayer disintegration. *Chem. Phys. Lett.* 486:99–103.
10. Boonnoy, P., V. Jarerattanachat, …, J. Wong-Ekkabut. 2015. Bilayer deformation, pores, and micellation induced by oxidized lipids. *J. Phys. Chem. Lett.* 6:4884–4888.
11. Van der Paal, J., E. C. Neyts, …, A. Bogaerts. 2016. Effect of lipid peroxidation on membrane permeability of cancer and normal cells subjected to oxidative stress. *Chem. Sci.* 7:489–498.
12. Bacellar, I. O. L., M. C. Oliveira, …, M. S. Baptista. 2018. Photosensitized membrane permeabilization requires contact-dependent reactions between photosensitizer and lipids. *J. Am. Chem. Soc.* 140:9606–9615.
13. Schumann-Gillett, A., and M. L. O'Mara. 2019. The effects of oxidised phospholipids and cholesterol on the biophysical properties of POPC bilayers. *Biochim. Biophys. Acta Biomembr.* 1861:210–219.
14. Boonnoy, P., M. Karttunen, and J. Wong-Ekkabut. 2017. Alpha-tocopherol inhibits pore formation in oxidized bilayers. *Phys. Chem. Chem. Phys.* 19:5699–5704.
15. Wang, T. Y., M. D. J. Libardo, …, J. P. Pellois. 2017. Membrane oxidation in cell delivery and cell killing applications. *ACS Chem. Biol.* 12:1170–1182.
16. Libardo, M. D. J., T. Y. Wang, …, A. M. Angeles-Boza. 2017. How does membrane oxidation affect cell delivery and cell killing? *Trends Biotechnol.* 35:686–690.
17. Keidar, M. 2015. Plasma for cancer treatment. *Plasma Sources Sci. Technol.* 24:033001.
18. Agmon, E., J. Solon, …, B. R. Stockwell. 2018. Modeling the effects of lipid peroxidation during ferroptosis on membrane properties. *Sci. Rep.* 8:5155.
19. Owen, M. C., W. Kulig, …, B. Strodel. 2018. Cholesterol protects the oxidized lipid bilayer from water injury: an all-atom molecular dynamics study. *J. Membr. Biol.* 251:521–534.
20. Kulig, W., A. Olżyńska, …, P. Jungwirth. 2015. Cholesterol under oxidative stress-how lipid membranes sense oxidation as cholesterol is being replaced by oxysterols. *Free Radic. Biol. Med.* 84:30–41.
21. Khandelia, H., B. Loubet, …, M. Hof. 2014. Pairing of cholesterol with oxidized phospholipid species in lipid bilayers. *Soft Matter.* 10:639–647.
22. Kerdous, R., J. Heuvingh, and S. Bonneau. 2011. Photo-dynamic induction of oxidative stress within cholesterol-containing membranes: shape transitions and permeabilization. *Biochim. Biophys. Acta.* 1808:2965–2972.
23. Sheetz, M. P., and S. J. Singer. 1974. Biological membranes as bilayer couples. A molecular mechanism of drug-erythrocyte interactions. *Proc. Natl. Acad. Sci. USA.* 71:4457–4461.
24. Bennett, W. F., J. L. MacCallum, …, D. P. Tieleman. 2009. Molecular view of cholesterol flip-flop and chemical potential in different membrane environments. *J. Am. Chem. Soc.* 131:12714–12720.
25. Jo, S., H. Rui, …, W. Im. 2010. Cholesterol flip-flop: insights from free energy simulation studies. *J. Phys. Chem. B.* 114:13342–13348.
26. Bennett, W. F. D., and D. P. Tieleman. 2012. Molecular simulation of rapid translocation of cholesterol, diacylglycerol, and ceramide in model raft and nonraft membranes. *J. Lipid Res.* 53:421–429.
27. Thallmair, S., H. I. Ingólfsson, and S. J. Marrink. 2018. Cholesterol flip-flop impacts domain registration in plasma membrane models. *J. Phys. Chem. Lett.* 9:5527–5533.

28. Gu, R. X., S. Baoukina, and D. P. Tieleman. 2019. Cholesterol flip-flop in heterogeneous membranes. *J. Chem. Theory Comput.* 15:2064–2070.
29. Smith, L. L. 1991. Another cholesterol hypothesis: cholesterol as antioxidant. *Free Radic. Biol. Med.* 11:47–61.
30. Parasassi, T., A. M. Giusti, …, E. Gratton. 1995. Cholesterol protects the phospholipid bilayer from oxidative damage. *Free Radic. Biol. Med.* 19:511–516.
31. Van der Paal, J., C. Verheyen, …, A. Bogaerts. 2017. Hampering effect of cholesterol on the permeation of reactive oxygen species through phospholipids bilayer: possible explanation for plasma cancer selectivity. *Sci. Rep.* 7:39526.
32. Boonnoy, P., M. Karttunen, and J. Wong-Ekkabut. 2018. Does α-tocopherol flip-flop help to protect membranes against oxidation? *J. Phys. Chem. B.* 122:10362–10370.
33. de Almeida, R. F., J. Borst, …, A. J. Visser. 2007. Complexity of lipid domains and rafts in giant unilamellar vesicles revealed by combining imaging and microscopic and macroscopic time-resolved fluorescence. *Biophys. J.* 93:539–553.
34. Mills, T. T., G. E. Toombes, …, J. F. Nagle. 2008. Order parameters and areas in fluid-phase oriented lipid membranes using wide angle x-ray scattering. *Biophys. J.* 95:669–681.
35. Alwarawrah, M., J. Dai, and J. Huang. 2010. A molecular view of the cholesterol condensing effect in DOPC lipid bilayers. *J. Phys. Chem. B.* 114:7516–7523.
36. Leeb, F., and L. Maibaum. 2018. Spatially resolving the condensing effect of cholesterol in lipid bilayers. *Biophys. J.* 115:2179–2188.
37. Vist, M. R., and J. H. Davis. 1990. Phase equilibria of cholesterol/dipalmitoylphosphatidylcholine mixtures: 2H nuclear magnetic resonance and differential scanning calorimetry. *Biochemistry.* 29:451–464.
38. Waheed, Q., R. Tjörnhammar, and O. Edholm. 2012. Phase transitions in coarse-grained lipid bilayers containing cholesterol by molecular dynamics simulations. *Biophys. J.* 103:2125–2133.
39. Wang, Y., P. Gkeka, …, Z. Cournia. 2016. DPPC-cholesterol phase diagram using coarse-grained molecular dynamics simulations. *Biochim. Biophys. Acta.* 1858:2846–2857.
40. Lee, S., D. W. Jeong, and M. C. Choi. 2017. Vertical order of DPPC multilayer enhanced by cholesterol-induced ripple-to-liquid ordered (LO) phase transition: synchrotron x-ray reflectivity study. *Curr. Appl. Phys.* 17:392–397.
41. Bennett, W. F. D., J. E. Shea, and D. P. Tieleman. 2018. Phospholipid chain interactions with cholesterol drive domain formation in lipid membranes. *Biophys. J.* 114:2595–2605.
42. Munro, S. 2003. Lipid rafts: elusive or illusive? *Cell.* 115:377–388.
43. Simons, K., and E. Ikonen. 1997. Functional rafts in cell membranes. *Nature.* 387:569–572.
44. de Meyer, F., and B. Smit. 2009. Effect of cholesterol on the structure of a phospholipid bilayer. *Proc. Natl. Acad. Sci. USA.* 106:3654–3658.
45. Bachar, M., P. Brunelle, …, A. Rauk. 2004. Molecular dynamics simulation of a polyunsaturated lipid bilayer susceptible to lipid peroxidation. *J. Phys. Chem. B.* 108:7170–7179.
46. Höltje, M., T. Förster, …, H. D. Höltje. 2001. Molecular dynamics simulations of stratum corneum lipid models: fatty acids and cholesterol. *Biochim. Biophys. Acta.* 1511:156–167.
47. Knight, C. J., and J. S. Hub. 2015. MemGen: a general web server for the setup of lipid membrane simulation systems. *Bioinformatics.* 31:2897–2899.
48. Abraham, M. J., T. Murtola, …, E. Lindahl. 2015. GROMACS: high performance molecular simulations through multi-level parallelism from laptops to supercomputers. *SoftwareX.* 1–2:19–25.
49. Bussi, G., D. Donadio, and M. Parrinello. 2007. Canonical sampling through velocity rescaling. *J. Chem. Phys.* 126:014101.
50. Parrinello, M., and A. Rahman. 1981. Polymorphic transitions in single crystals: a new molecular dynamics method. *J. Appl. Phys.* 52:7182–7190.
51. Hess, B. 2008. P-LINCS: a parallel linear constraint solver for molecular simulation. *J. Chem. Theory Comput.* 4:116–122.
52. Wong-Ekkabut, J., and M. Karttunen. 2016. The good, the bad and the user in soft matter simulations. *Biochim. Biophys. Acta.* 1858:2529–2538.
53. Darden, T., D. York, and L. Pedersen. 1993. Particle mesh Ewald: an N· log (N) method for Ewald sums in large systems. *J. Chem. Phys.* 98:10089–10092.
54. Essmann, U., L. Perera, …, L. G. Pedersen. 1995. A smooth particle mesh Ewald method. *J. Chem. Phys.* 103:8577–8593.
55. Karttunen, M., J. Rottler, …, C. Sagui. 2008. Electrostatics in biomolecular simulations: where are we now and where are we heading? *Curr. Top. Membr.* 60:49–89.
56. Wong-Ekkabut, J., and M. Karttunen. 2016. Molecular dynamics simulation of water permeation through the alpha-hemolysin channel. *J. Biol. Phys.* 42:133–146.
57. Kongsema, M., S. Wongkhieo, …, J. Wong-Ekkabut. 2019. Molecular mechanism of Forkhead box M1 inhibition by thiostrepton in breast cancer cells. *Oncol. Rep.* 42:953–962.
58. Enkavi, G., M. Javanainen, …, I. Vattulainen. 2019. Multiscale simulations of biological membranes: the challenge to understand biological phenomena in a living substance. *Chem. Rev.* 119:5607–5774.
59. Nalakarn, P., P. Boonnoy, …, J. Wong-Ekkabut. 2019. Dependence of fullerene aggregation on lipid saturation due to a balance between entropy and enthalpy. *Sci. Rep.* 9:1037.
60. Khuntawee, W., T. Sutthibutpong, …, J. Wong-Ekkabut. 2019. Molecular dynamics study of natural rubber-fullerene composites: connecting microscopic properties to macroscopic behavior. *Phys. Chem. Chem. Phys.* 21:19403–19413.
61. Nisoh, N., V. Jarerattanachat, …, J. Wong-Ekkabut. 2020. Formation of aggregates, icosahedral structures and percolation clusters of fullerenes in lipids bilayers: the key role of lipid saturation. *Biochim. Biophys. Acta Biomembr.* 1862:183328.
62. Khuntawee, W., R. Amornloetwattana, …, J. Wong-ekkabut. 2021. In silico and in vitro design of cordycepin encapsulation in liposomes for colon cancer treatment. *RSC Adv.* 11:8475–8484.
63. Humphrey, W., A. Dalke, and K. Schulten. 1996. VMD: visual molecular dynamics. *J. Mol. Graph.* 14:33–38.
64. Torrie, G. M., and J. P. Valleau. 1977. Nonphysical sampling distributions in Monte Carlo free-energy estimation: umbrella sampling. *J. Comput. Phys.* 23:187–199.
65. Kumar, S., J. M. Rosenberg, …, P. A. Kollman. 1992. The weighted histogram analysis method for free-energy calculations on biomolecules. I. The method. *J. Comput. Chem.* 13:1011–1021.
66. Watkins, J. C. 2016. An Introduction to the Science of Statistics: From Theory to Implementation, Preliminary Edition: The University of Arizona, Arizona, math.arizona.edu/∼jwatkins/statbook.pdf.
67. Garrec, J., A. Monari, …, M. Tarek. 2014. Lipid peroxidation in membranes: the peroxyl radical does not "float". *J. Phys. Chem. Lett.* 5:1653–1658.
68. Rosa, R., F. Spinozzi, and R. Itri. 2018. Hydroperoxide and carboxyl groups preferential location in oxidized biomembranes experimentally determined by small angle x-ray scattering: Implications in membrane structure. *Biochim. Biophys. Acta Biomembr.* 1860:2299–2307.
69. Israelachvili, J. N., D. J. Mitchell, and B. W. Ninham. 1976. Theory of self-assembly of hydrocarbon amphiphiles into micelles and bilayers. *J. Chem. Soc. Faraday Trans. II.* 72:1525–1568.
70. Hub, J. S., F. K. Winkler, …, B. L. de Groot. 2010. Potentials of mean force and permeabilities for carbon dioxide, ammonia, and water flux across a Rhesus protein channel and lipid membranes. *J. Am. Chem. Soc.* 132:13251–13263.
71. Choubey, A., R. K. Kalia, …, P. Vashishta. 2013. Cholesterol translocation in a phospholipid membrane. *Biophys. J.* 104:2429–2436.

72. Ermilova, I., and A. P. Lyubartsev. 2018. Cholesterol in phospholipid bilayers: positions and orientations inside membranes with different unsaturation degrees. *Soft Matter.* 15:78–93.

73. Sankaram, M. B., and T. E. Thompson. 1991. Cholesterol-induced fluid-phase immiscibility in membranes. *Proc. Natl. Acad. Sci. USA.* 88:8686–8690.

74. de Almeida, R. F., and E. Joly. 2014. Crystallization around solid-like nanosized docks can explain the specificity, diversity, and stability of membrane microdomains. *Front Plant Sci.* 5:72.

75. Róg, T., M. Pasenkiewicz-Gierula, …, M. Karttunen. 2009. Ordering effects of cholesterol and its analogues. *Biochim. Biophys. Acta.* 1788:97–121.

76. Marrink, S. J., A. H. De Vries, and A. E. Mark. 2004. Coarse grained model for semiquantitative lipid simulations. *J. Phys. Chem. B.* 108:750–760.

77. Yan, D., J. H. Sherman, and M. Keidar. 2017. Cold atmospheric plasma, a novel promising anti-cancer treatment modality. *Oncotarget.* 8:15977–15995.